FRICTION STIR WELDING OF ALUMINIUM BASED COMPOSITES REINFORCED WITH AL_2O_3 PARTICLES: EFFECTS ON MICROSTRUCTURE AND CHARPY IMPACT ENERGY

[1]Iuri Boromei, [1]Lorella Ceschini, [1]Alessandro Morri, [2]Gian Luca Garagnani
[1]SMETEC Department, University of Bologna, Bologna
[2]Department of Engineering, University of Ferrara, Ferrara

Abstract

The aim of the present research was to study the effect of the Friction Stir Welding process on the microstructure and impact toughness of the composites W6A20A (AA6061 reinforced with 20vol.% of Al_2O_3 particles) and W7A10A (AA7005 reinforced with 10vol.% of Al_2O_3 particles).

FSW, because of the concurrent effect of severe plastic deformation and frictional heating during welding, had effects both on the reinforcing particles and the aluminium matrix. It induced a significant reduction in the reinforcement particles size and their better distribution in the welded zone as well as a grain refinement of the aluminium alloy matrix in the nugget due to dynamic recrystalizzation. The frictional heating, moreover, had effects on the growth, dissolution and re-precipitation of hardening precipitates.

The impact tests showed that the total impact energies increased in the FSW composites, respect to the corresponding base materials.

Riassunto

In questa ricerca è stato studiato l'effetto della Friction Stir Welding sulla microstruttura e sulla resilienza dei compositi Duralcan W6A20A e W7A10A, aventi come matrici le leghe AA6061 e AA7005 rinforzate con il 20% e 10% in volume, rispettivamente, di particelle di Al_2O_3. I risultati della caratterizzazione microstrutturale hanno evidenziato come il processo FSW, in conseguenza dei campi termici e di deformazione plastica indotti, abbia effetti sia sulla matrice, che sulle particelle di rinforzo. In entrambi i compositi l'utensile ha indotto una frammentazione delle particelle di maggiori dimensioni, un arrotondamento degli spigoli ed una migliore distribuzione delle stesse nel cordone, rispetto al materiale base. A seguito di fenomeni di ricristallizzazione dinamica, si è osservato un affinamento dei grani della matrice nel *nugget*; mentre per quanto riguarda i precipitati indurenti, i campi termici hanno indotto fenomeni di ingrossamento, dissoluzione e riprecipitazione di diversa entità nelle varie zone del cordone.

Le modificazioni microstrutturali hanno portato ad un incremento significativo dei valori di resilienza dei campioni sottoposti a FSW rispetto ai valori rilevati nei compositi non saldati.

INTRODUCTION

Aluminium matrix composites, reinforced with ceramic particles, can be welded by fusion processes and solid state joint processes [1]. However, the traditional fusion welding techniques should be critical when applied to these materials. Some difficulties are associated with the typical welding problems of aluminium alloys, such as: high thermal expansion and conductivity, high solubility of gases in the molten state, solidification shrinkages and cracking presence of oxide inclusions. Moreover, the presence of the ceramic reinforcement can cause other problems, making welding difficult, such as: high viscosity of the melted composites respect to the unreinforced alloys, that leads to an extensive presence of solidification shrinkages and porosity; undesired interfacial chemical reactions between the ceramic reinforcement and the molten matrix alloy; different thermal expansion coefficients between the matrix and the ceramic reinforcement, which cause thermal stresses during welding; segregation of particles during solidification, with a consequent reduction in the mechanical properties.
Friction Stir Welding (FSW) is a relatively new joining process, developed at The Welding Institute (TWI) in 1991 for aluminium alloys, and is presently attracting considerable interest [2-5]. In this solid state welding technique (schematically showed in Fig.1 [6]) a rotating tool, cylindrical in shape with a pin of smaller diameter extending from the tool shoulder, is translated along the joint line and produces, during its path, frictional heating and also plastic deformation of the material, due to a stirring effect around the pin. The material along the joint line is heated to a softened condition, transferred around the periphery of the tool, and subsequently solid state welded. Important process parameters include the tool geometry, the rpm and travel speed, as well as the downward force on the tool.
Friction Stir Welding has been initially developed for welding aluminium alloys, but several recent studies show that it should be also successfully applied to other materials, such as particles reinforced aluminium based composites [7-9]. In this case, wear damage of the tool occurs during welding, due to the abrasive action of the ceramic reinforcement [10]. However, since joining occurs in the solid state, FSW, respect to the classic fusion welding techniques, avoids the formation of shrinkages, porosity as well as the aggregation of the ceramic reinforcement in the welded zone and significantly reduces the thermal stresses.
The aim of the present research was to study the effect of the FSW process on the microstructure and impact toughness of two aluminium matrix composites, based on the AA6061 reinforced with 20vol.% of Al_2O_3 particles (W6A20A) and on the AA7005 reinforced with 10vol.% of Al_2O_3 particles (W7A10A). The impact behaviour was studied using an instrumented Charpy impact pendulum and the results were related to the microstructure modifications induced by the FSW.

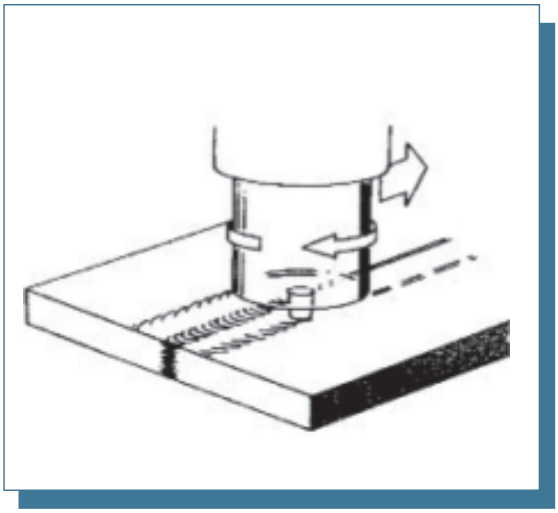

Fig. 1: Schematic representation of the FSW process for butt joint welding. The FSW tool is rotated and traversed along the joint to produce the weld [13].

EXPERIMENTAL

The W6A20A and W7A10A composites were produced by Duralcan (USA) using a proprietary molten metal processing. The as-cast composites were extruded at 480 °C to a rectangular plate (cross section of 100x7 mm^2) and then were heat treated at the T6 state, including: solubilization at 540 °C for 1 h, water quenching and ageing at 145°C for 16 h, for the W6A20A; solubilization at 465 °C for 1 h, water quenching and aging at 95 °C for 1h and 145 °C for 16 h, for the W7A10A.
The extruded and T6 treated plates (7 mm in thickness) were Friction Stir Welded at the GKSS Research Institute (Geesthacht, Germany), by using a Neos Triceps 805, CN controlled, five-axis robot [8]. The FSW tool (showed in Fig.2), with 20 mm diameter shoulder and 8 mm diameter pin, was made with a highly wear resistant steel (an age-hardenable martensite reinforced with 30vol.% TiC), having a hardness of about 63 HRC.
The microstructural characterization of welded composites, was carried out by means of optical (OM) and scanning electron microscopy (SEM) equipped with an energy dispersive spectroscopy (EDS). Image analyses, performed with the Image Pro-Plus software, were carried out on the optical micrographs, in order to evaluate the effect of the FSW process on the reinforcement particles (size, shape and local volume fraction) and on the aluminium matrix grain size. The effect of the FSW process on the particles distribution was also

Fig. 2: Threaded tool used for the FSW process [14].

studied by means of the Voronoi tessellation method [11-12]. According to this statistic method, given a set of points (called generators) and a distance function, Voronoi tessellations are subdivisions of another set of points into subsets such that the points in each subset are closest, with respect to the given distance function, to one of the generators than to any of the other generators. Voronoi tessellation is useful in very different applications: simulation of grain growth damage and shear banding in polycrystals, characterisation of composites and simulation of microcrack nucleation or intergranular stress corrosion.

For metallographic investigations the specimens were mechanically ground on coarse emery papers, then polished with 9, 6 and 1 μm diamond paste and finally etched with Keller's reagent.

Microhardness profiles were taken across the welded joint. A 20 g load was used for the Vickers indentation ($HV_{0.02}$), in order to evaluate only the matrix interparticles microhardness.

The impact tests were carried out on welded and base composites (five specimens for each material), using an instrumented pendulum machine (CEAST, Resil Impactor 50 J), according to ASTM E 23. Sub-size Charpy V specimens (10x5x55 mm^3, with 2 mm deep V-notch) were used for the tests, due to the reduced thickness of the plates; the specimens were electro-discharge machined with the notch perpendicular to the welded line (Fig.3). In order to investigate the influence of the FSW process on the mechanisms of failure of the tested composites, SEM analyses were carried out on the fracture surfaces.

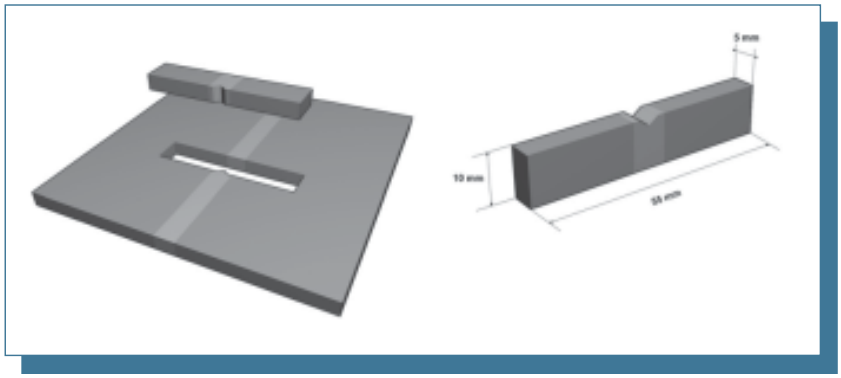

Fig. 3: Scheme of the machining of the Charpy specimens from the FSW plates and dimensions of the sub-size specimens used for the tests.

RESULTS AND DISCUSSION

Microstructural characterization

The Fig. 4 shows a friction stir welded composite plates. The surface in contact with the tool shoulder (Fig.4-a) is characterized by the presence of semicircular features, similar to those induced by a conventional milling process. The average surface roughness Ra on this side, evaluated by a stylus profilometer along the y-direction (according to the scheme in Fig.5), was equal to 3.5 μm. The opposite surface (Fig.4-b) doesn't show evident surface modification induced by the FSW process and so the average surface roughness was the same of the base material (as received) (Ra=0.7 μm).

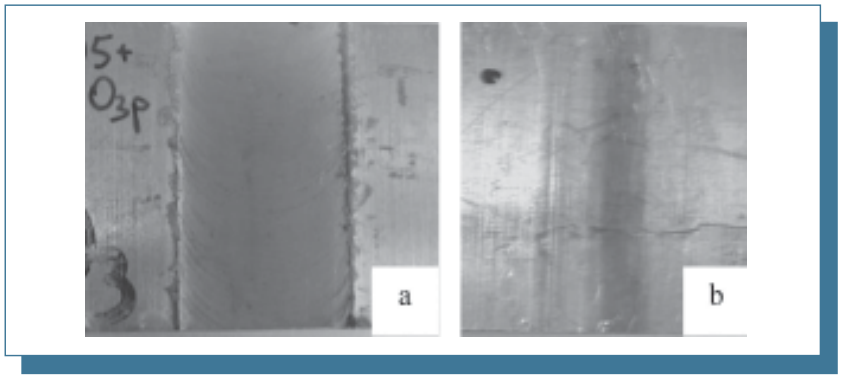

Fig. 4: Friction Stir Welded composite plate: surface in contact with the shoulder (a) and opposite side (b).

The microstructural characterization was carried out on samples cut from the transverse cross section of the welded plate, at different y-values (according to Fig.5), that is from the base material to the nugget zone (welded zone), and at different z-values, that is at different distances from the shoulder tool. Figure 6 is a typical low magnification optical image of the welded zone, showing the "onion ring" structure characteristic of the FSW. None of the typical defects, generally observed in the welded zone of MMCs joined using conventional melting processes, such as porosity or reinforcement segregation, was detected. Optical micrographs showing the transition from the base material (left side) to the nugget (right side) are shown in Fig.7 (*a-b*) for the W6A20A and W7A10A, respectively. In both materials, a different distribution of particles and a reduction in their size, due to the abrasive action of the hard tool, are evident. Fragmentation of the large alumina particles, induced by the FSW, was confirmed by the image analyses, carried out on optical micrographs of the base and welded materials. The results, reported in Table I, show that the particles refinement was higher for the W6A20A, characterized by initial larger reinforcement particles (average particle area =135 μm^2), respect to those of the W7A10A (average particle area = 44 μm^2). The particle area, in the welded W6A20A, decreased of about 60% and 40%, in zones closer or farther from the shoulder respectively, probably due to different stresses induced by the

tool on the particles and to the highest contact area between the tool and the material, due to the tool geometry. In this composite, also the particle shape factor was reduced by the FSW process, from 2.1 in the base material to 1.9 in the FSW zone. It is worth noting that the variations in the reinforcement size and shape should reduce the stress intensification caused by the particles, enhancing the toughness of the welded composite. A reduction in the particles area (about 30%) and no variation in the particle shape factor were, instead, observed in the W7A10A composite, probably due to the smaller initial size of the reinforcement particles.
Several authors report that FSW also leads to dynamic recrystallization of aluminium alloys, due to severe plastic deformation producing large frictional heating [13-15]. This effect is enhanced by the reinforcement particles, stimulating nuclei for recrystallization [16]. A substantial grain refinement in the aluminium alloy matrix, in fact, was observed in the nugget of both welded composites, as one can see by comparing the microstructures of the base materials and nugget zones (Fig.8). The average grain size of the aluminium alloy matrix, in the W6A20A, decreased from about 29 μm in the base material to 20 μm in the FSW zone. A superior grain refinement was observed in the W7A10A, that showed a decrease of the aluminium matrix grain size from 29 μm in the base material to 12 μm in the nugget zone.
It is well known that a homogeneous distribution of the reinforcement particles is one of the main requirements to achieve good mechanical properties in discontinuously reinforced composites. Therefore, it is important that the welding process doesn't lead to particle clusters or particle denuded zones. Among the various methods for characterising second phase distributions, tessellation methods have attracted particular attention in their ability to uniquely characterise the surroundings of individual particles within a distribution. The Voronoi tessellation method, in particular, utilizes the centre of the particles to construct a network of polygonal cells, such that any point within a cell is closer to the centre of the particle than to any other centre [11-12]. In particles reiforced composites, with a perfect distribution of the reinforcement, the ratio between the particles area and its area of influence in the matrix, should be equal to the volume fraction of the reinforcement. Therefore the Voronoi tessellation should be a useful method to evaluate the degree of clustering in these composites [17]. In this work, the Voronoi tessellation was used to evaluate the effect of the Friction Stir Welding on the reinforcement particles distribution. The results of the statistical analyses, carried out on the W6A20A and

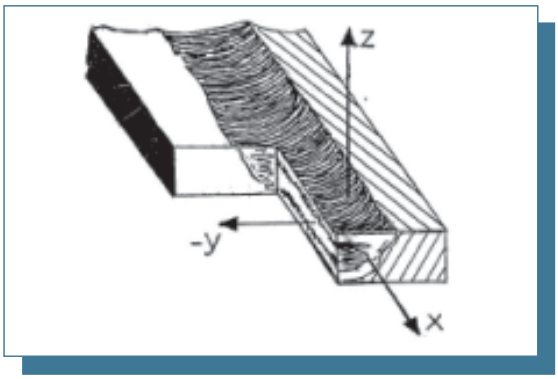

Fig. 5: Schematization of the FSW cross section.

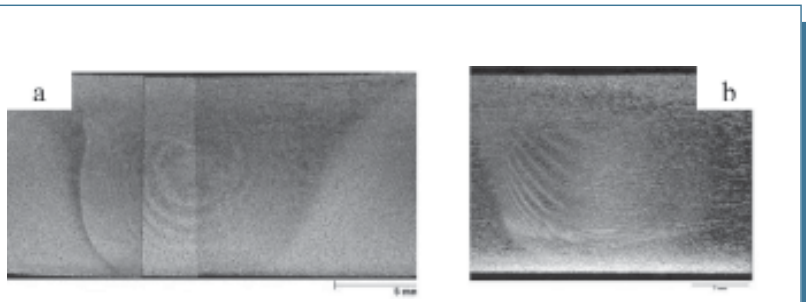

Fig. 6: Optical micrographs with macroscopic features of the cross sections of the W6A20A (a) and W7A10A (b) FSW composites.

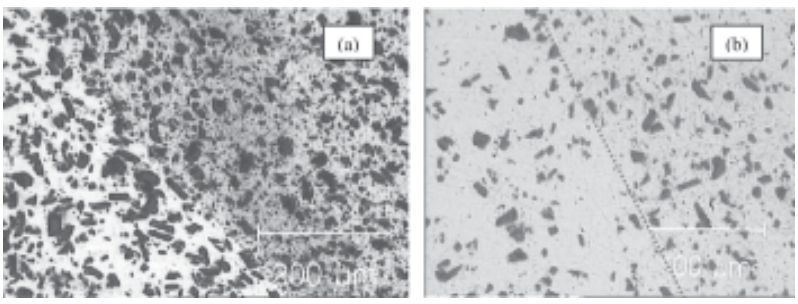

Fig. 7: Optical micrographs of the cross-sections of the FSW plates (y-direction): transition from the base materials (left side) and the advancing side of the FSW zones (right side) for the W6A20A (a) and the W7A10A (b).

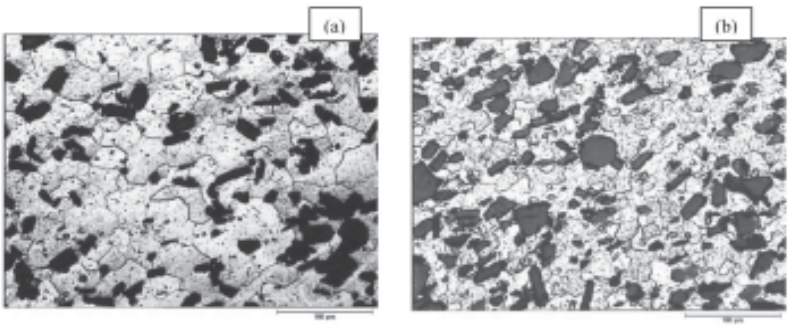

Fig. 8: Effect of FSW on the aluminium matrix grain size, for the W6A20A: base material (a) and nugget (b).

W7A10A, are reported in Figs.9-11, respectively. It can be noted that, consequently to the abrasion and fragmentation of the reinforcement particles, caused by the tool and the following increase in their number, the polygons area decreased, then also decreased the area of influence of each reinforcement particle. The plots in Fig.10 and Fig.11 show that the FSW process also led to a decrease in the standard deviation of the local reinforcement volume fraction, respect to the base material, indicating a more uniform distribution of the particles. This reduction was equal to about 26% in the W6A20A composite and about 67% in the W7A10A, suggesting that the final microstructure of the latter composite extend to the random model. This result should be probably due to the lower reinforcement content, in the W7A10A, that permits a superior stirring effect of the pin into the 7005 aluminium alloy matrix.

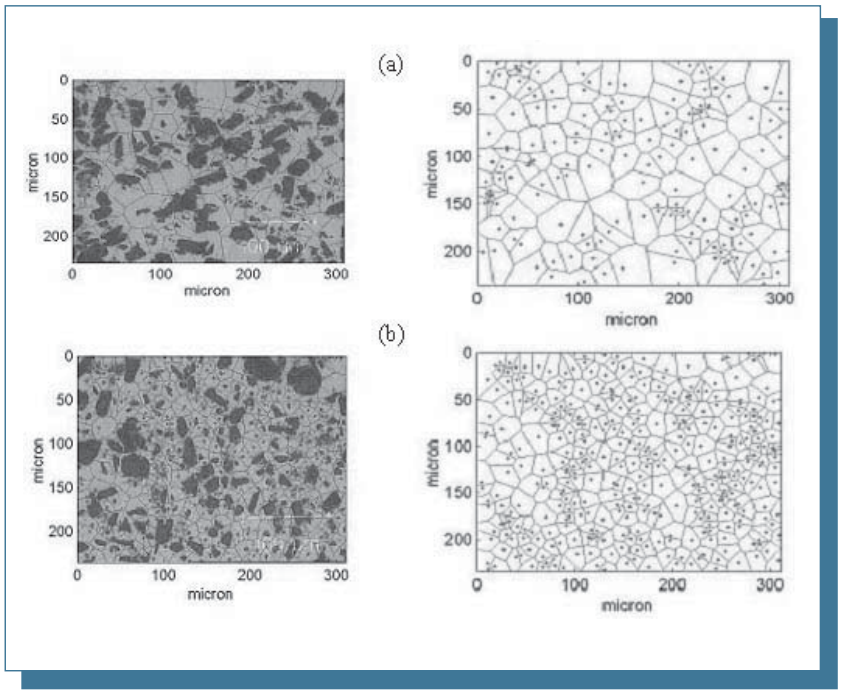

Fig. 9: Voronoi Tessellation carried out on the base material (a) and FSW zone (b) of the W6A20A composite.

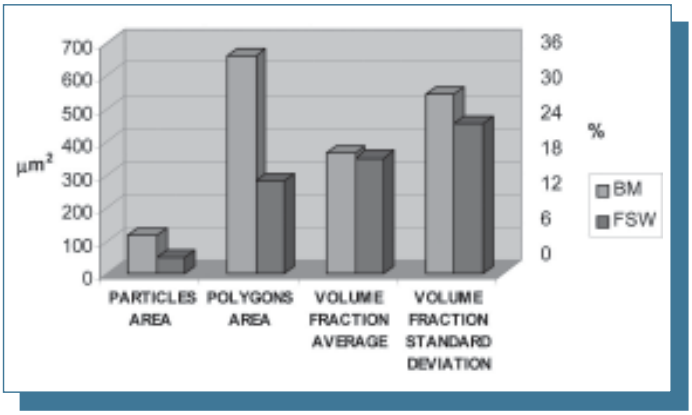

Fig. 10: Results of the Voronoi Tessellation carried out on the base and FSW W6A20A composite.

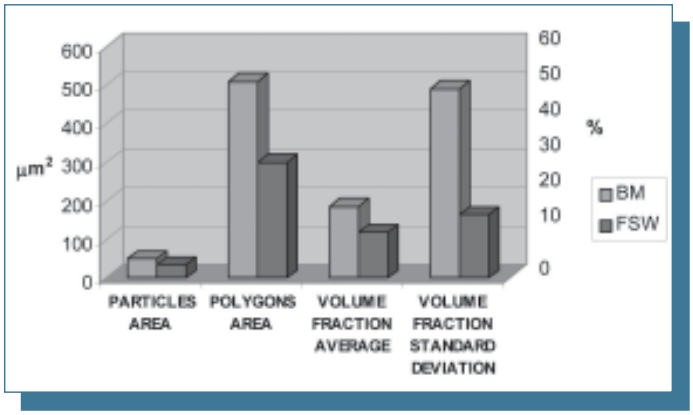

Fig. 11: Results of the Voronoi Tessellation carried out on the base and FSW W7A10A composite.

Microhardness measurements

In order to investigate softening or hardening effects induced by the FSW process on the aluminium matrix alloys, microhardness measurements, with a very low load ($HV_{0.02}$), were made from the base material to the nugget zone, on cross-sections of the welded plates. The results are shown in the plots of Fig.12(*a*) for the W6A20A, and Fig.12(*b*) for the W7A10A.

The microhardness profile of the W6A20A shows a decrease of the interparticles matrix microhardness from about 80 $HV_{0.02}$ in the base material up to about 50 $HV_{0.02}$ at the middle line of the FSW zone. This microhardness decrease in the aluminium alloy matrix, even with a reduction in its grain size, was also observed in FSW unreinforced AA6061 and should be probably related to coarsening or partial dissolution of the intermetallic compounds, induced by the frictional heating and severe plastic deformation [18,19]. The microhardness profile for the W7A10A, in Fig.12(*b*), shows a minimum value of about 77 $HV_{0.02}$ at the middle line of the nugget zone, a maximum value of about 100 $HV_{0.02}$ in the thermomechanical affected (TMAZ) zone, a second minimum of about 75 $HV_{0.02}$ in the heat affected zone (HAZ); then, the interparticles matrix microhardness increased up to about 84 $HV_{0.02}$ in the base material. This trend can be also related to the microstructural changes induced by the friction stir welding process on the aluminium alloy matrix. In particular, the observed maximum in the TMAZ is probably due to the concurrent effects of strain-hardening and re-precipitation of the transition phases; the lower microhardness in the nugget should be related to

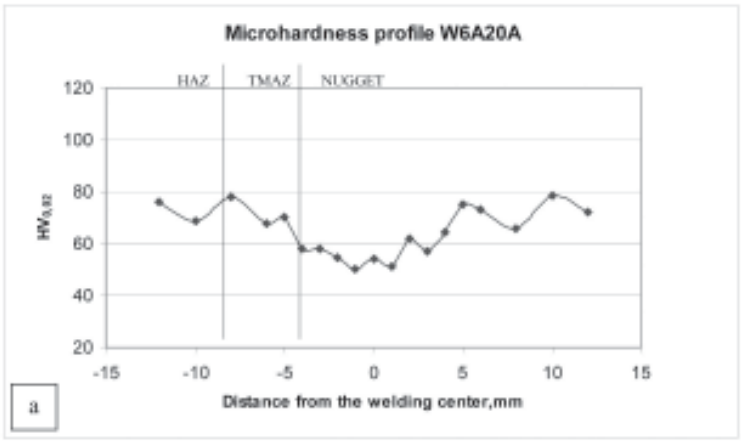

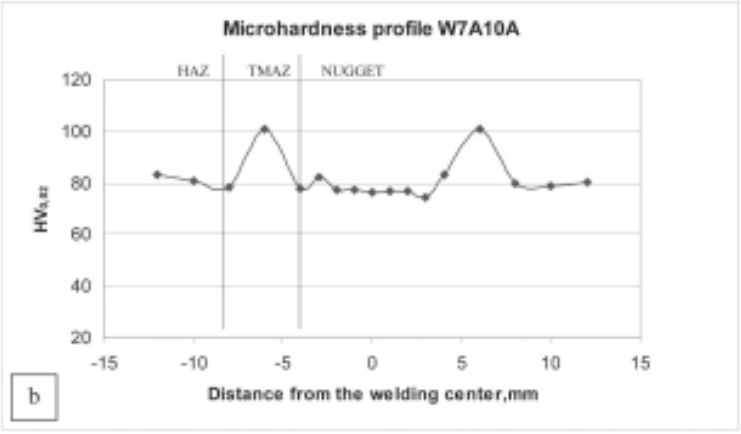

Fig. 12: Microhardness profiles on the cross sections of the FSW composites: W6A20A (a) and W7A10A (b).

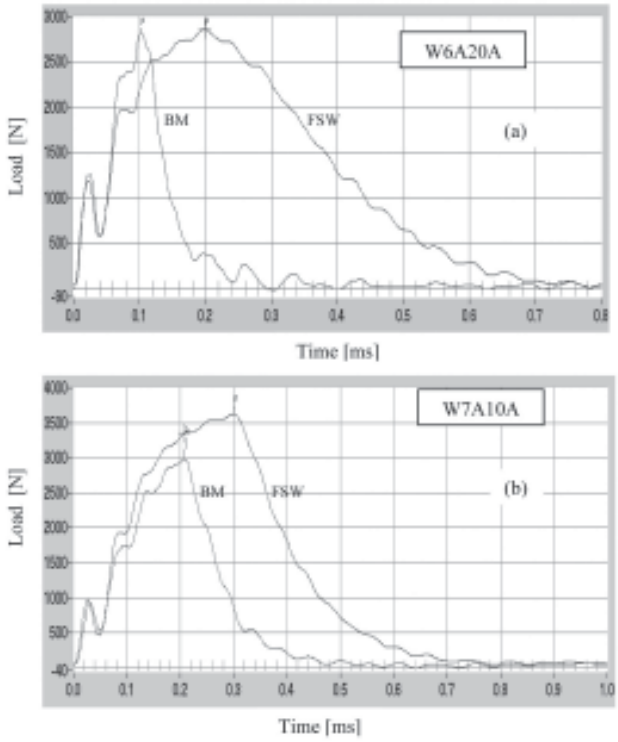

Fig. 13: Comparison of the load *vs* time curves for the composites W6A20A (a) and the W7A10A (b): base material (BM) and Friction Stir Welded (FSW).

coarsening and/or dissolution of the precipitates and, finally, the minimum of microhardness in the HAZ may be caused by coarsening of the precipitates induced by the frictional heating [20-24]. The different interparticles microhardness profiles in the two FSW composites is therefore due both to the different aluminium matrix grain size, induced by dynamic recrystallization in the nugget, and to the different aging response of the matrix alloys during and after welding.

Instrumented Charpy Impact Tests

Impact tests were carried on the sub-size specimens shown in Fig.3, using an instrumented Charpy pendulum, to investigate the effect of the FSW process. The load-time curve (Fig. 13) can be divided into an elastic zone, corresponding to the initial rise of the curve, a plastic zone starting at the change of the curve slope and a crack zone, where the load rapidly decreases, indicating the start of the crack propagation. The first fluctuation in the rising side of the curve is caused by the inertial loading of the hammerhead, as a result of the acceleration of the specimen from rest. The total energy adsorbed by the specimen under fracture, given by the area under the load curve, is the sum of the energy required for crack initiation, Ei, and the energy required for crack propagation, Ep, and therefore gives the impact toughness of the tested material.

The results of the Charpy impact tests for the base and welded composites are reported in Table II (average values on five tests). Representative load-time curves for the base and welded materials are shown in Fig.13(*a*) for the W6A20A and Fig.13(*b*) for the W7A10A.

The impact energies increased in both the FSW composites, respect to the corresponding base materials, from 0.7 J to 2.6 J for the W6A20A composite, and from 1.2 J to 2.9 J for the W7A10A composite. This significant increase in the total adsorbed impact energies can be related to the microstructural modifications induced by the FSW process, such as: refinement and roundness of the reinforcement particles, homogeneous distribution of the reinforcement and reduction of the matrix grain size. In fact, it has been shown that ductility of particle reinforced aluminium alloys is reduced by the presence of large particles [25], but the particle size has little effect on ductility when particles are small [26]. Particle clusters in the matrix can also decrease ductility [27-28]. Also the effect of particle shape on fracture properties of the AA6061 matrix composites has been studied

[29-30] and it was found that, since stress concentration in the matrix increases around angular particles, tensile ductility of the composite will be reduced owing to the severe plastic deformation around the particle corners [30]. It is reasonable to suppose that reduction in size and blunting of the reinforcement particles should improve the impact toughness. In fact, it is reported that large and angular particles act as stress concentration sites and easy crack propagation, resulting in low impact toughness [31].
The increase in the crack initiation energy Ei and dynamic yield strength (Tab.II) are, probably, mainly related to the grain refinement of the matrix, that was of higher entity for the W7A10A (about 60%) respect to the W6A20A (about 30%). The histograms in Fig.14(*a-b*) show the contribution of the initiation (Ei) and propagation (Ep) energies to the total impact values, for the base and welded composites. The increase in the propagation energy was greater for the W6A20A, than for the W7A10A, and it is probably related to the higher reduction in the particles size (up to 60%) and particle shape-factor induced by the FSW in this composite, that mainly influence the crack propagation stage.

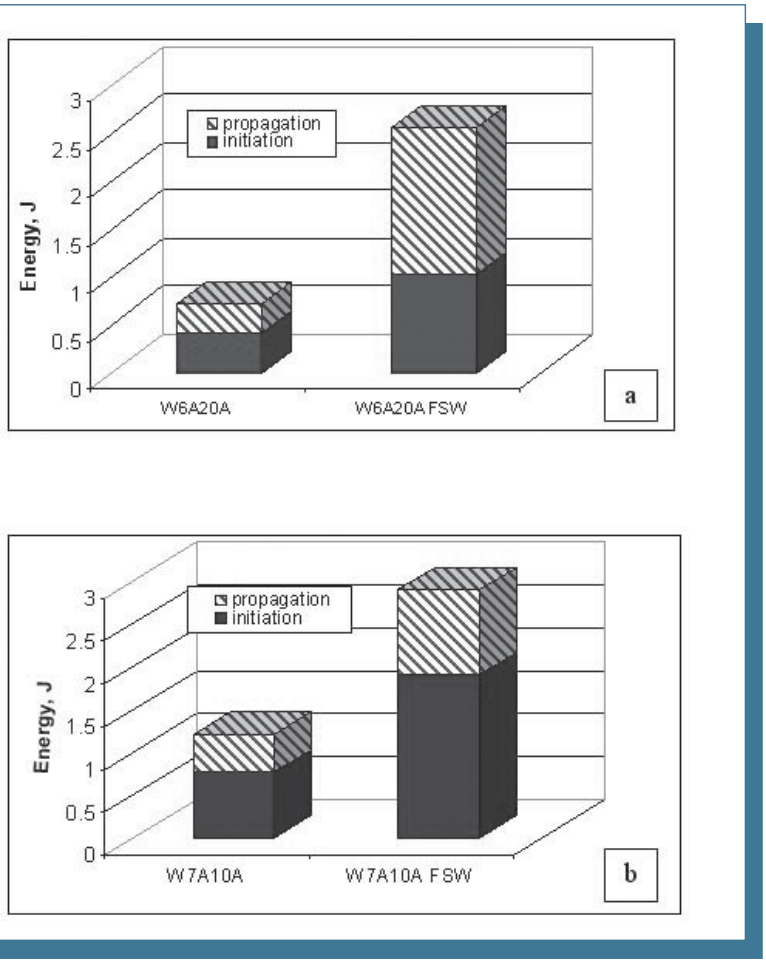

Fig. 14: Initiation and propagation energies for the base and FSW composites W6A20A (a) and W7A10A (b).

Fracture surfaces

Micrographs (Fig. 15) of the fractured Charpy specimen surfaces, show a greater amount of plastic deformation in the friction stir welded composites (Fig. 15 *b-d*), respect to the base materials (Fig. 15 *a-c*), clearly related to the increase in the total adsorbed energy.
This behaviour was confirmed by SEM analyses, which also permit to evidence more details on the mechanisms of fracture. Fracture surfaces of the impact specimens, machined from base and FSW composites, were always characterized by a bimodal distribution of voids, associated with decohesion of the reinforcement particles, and small dimples associated with the ductile failure of the matrix (Figs. 16 and 17).
In the welded W6A20A composite it is possible to observe a higher volume fraction of small voids, caused by decohesion of the reinforcing particles, and minute dimples, due to the plastic deformation of the matrix, than in the base composite (Fig. 16).

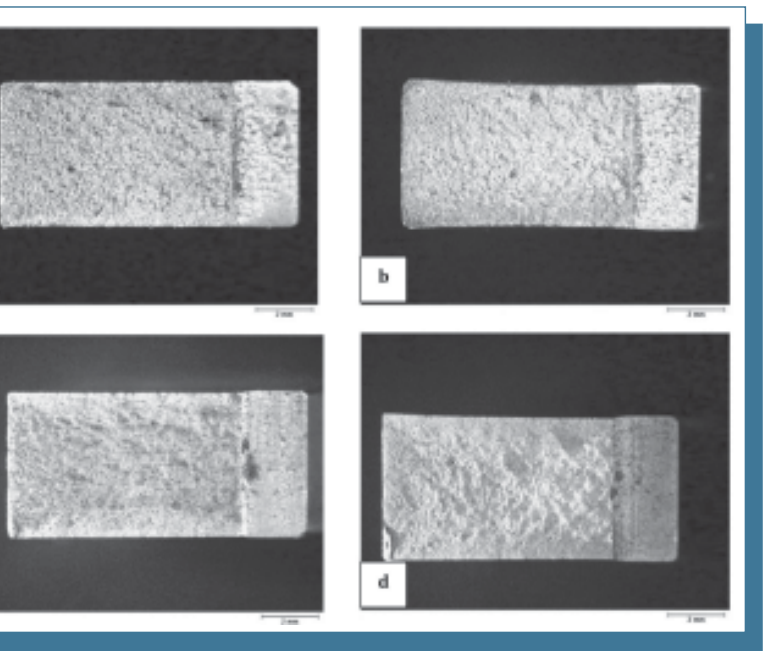

Fig. 15: Fracture surfaces at low magnification of Charpy impact specimens: base (a) and FSW (b) W6A20A composite; base (c) and FSW (d) W7A10A composite.

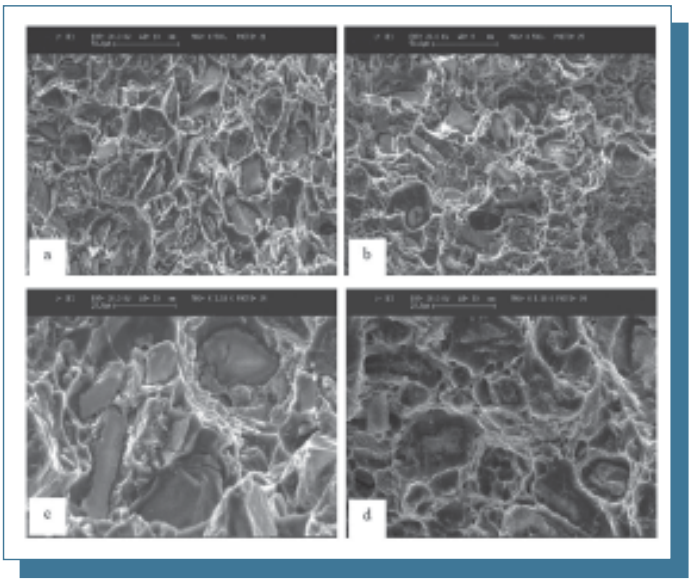

Fig. 16: SEM micrographs of the fracture surfaces of the Charpy impact specimens: base (a-c) and FSW (b-d) W6A20A composite.

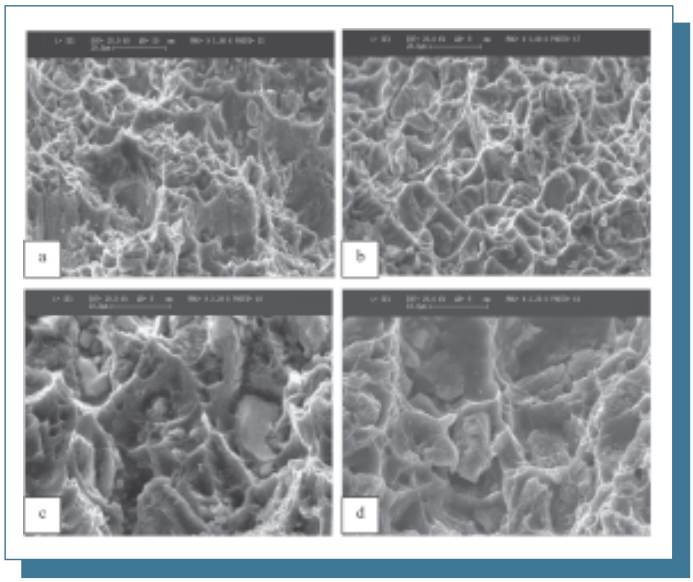

Fig. 17: SEM micrographs of the fracture surfaces of the Charpy impact specimens: base (a-c) and FSW (b-d) W7A10A composite.

Table 1 - Results of the image analyses measurements carried out on the reinforcement particles and matrix grain size of the W6A20A and W7A10A composite before and after FSW.

		Reinforcement particles				Matrix grain
Material	**Zone of analysis**	**Area μm²**	**Shape factor**	**Length μm**	**Width μm**	**Size μm**
W6A20A	Base Material	135	2.1	16	9	29
"	FSW zone farther	82	2.0	12	7	5
	from the shoulder tool					
"	FSW zone closer to	56	1.9	9	6	20
	the shoulder tool					
W7A10A	Base Material	44	2.2	9	5	29
"	FSW zone	30	2.1	8	4	12

Table 2 - Results of the instrumented Charpy impact tests on the base and FSW composites

Composite	**Total Impact Energy J**	**Initiation Energy J**	**Propagation Energy J**	**Dynamic yield strength MPa**
W6A20A BM	0.7	0.4	0.3	43
W6A20A FSW	2.6	1.0	1.6	48
W7A10A BM	1.2	0.8	0.4	38
W7A10A FSW	2.9	1.9	1.0	49

The higher presence of small voids and lower presence of cracked particles in the welded composite, can be explained with the reduction of local plastic constraints due to the reduction of particles size and better distribution of the reinforcement, induced by the welding process. The small dimensions of ductile dimples can be attributed to the constraints in plastic flow of the matrix, or to the reduction of strains and hence stresses, induced by the refined reinforcement [32-36]. These differences are not so evident for the W7A10A composite (Fig. 17), since the reinforcement particles are smaller in the base composite and their refinement after welding was lower than in the W6A20A (Table I). The larger presence of dimples in the fracture surfaces of the welded composites, especially in W6A20A, is in agreement with the significant increase in the Charpy impact toughness.

CONCLUSIONS

In this work the effect of the FSW process on the microstructure and impact toughness of two particles reinforced aluminium matrix composites (W6A20A and W7A10A) was investigated.

a) The microstructural characterization didn't show the typical defects generally observed in the welded zone of MMCs, joined using conventional arc welding processes. The main effects of the FSW was a significant reduction in the reinforcement particles size (greater in the W6A20A, due to the larger size of the particles in the base materials) and a more homogeneous distribution of the particles in the welded zone, as confirmed by the Voronoi tessellation analysis. A substantial grain refinement of the aluminium alloy matrix was also observed in the nugget of the welded zones, in both composites, due to dynamic recrystallization induced by the severe deformation and concurrent frictional heating during welding.

b) The interparticles microhardness profiles, on cross-sections of the FSW specimens, was related to the microstructural changes induced by the process on the aluminium alloy matrix. The differences between the two composites is due to the different aluminium matrix grain size, induced by dynamic recrystallization in the nugget, and to the different modifications of the intermetallic compounds.

c) The impact tests, carried out on an instrumented Charpy pendulum, showed that the total impact energy significantly increased in both the FSW composites, respect to the corresponding base materials. This increase can be related to the microstructural modifications induced by the FSW process, such as: refinement and blunting of the reinforcement particles, homogeneous distribution of the reinforcement and reduction in the matrix grain size.

d) Fracture surfaces of the impact specimens were always characterized by a bimodal distribution of voids, associated with decohesion of the reinforcement particles, and small dimples associated with the ductile failure of the matrix. The larger presence of dimples in the fracture surfaces of the welded composites, especially in W6A20A, is in agreement with the significant increase in the Charpy impact toughness.

REFERENCES

1. Ellis, M.B.D. Joining of aluminium based metal matrix composites. *International Materials Reviews*, 41 (1996), pp.41-58.
2. Miles, M.P., B.J. Decker and T.W. Nelson. Formability and Strength of Friction-Stir-Welded Aluminum Sheets. *Met and Mat Trans* A 35A (2004), pp.3461-3468.
3. Thomas, W.M. et al. Friction Stir Butt Welding. International Patent Appl. No. PCT/GB92/02203 and GB Patent Appl. No. 9125978.8, U.S. Patent No. 5460, 317 (1991).
4. Dawes, C. and Thomas W. *TWI Bulletin 6* (1995), p.124.
5. Ellis, M. and M. Strangwood. *TWI Bulletin 6* (1995), p.138.
6. Gould, J. E., Z. Feng and P. Ditzel. Preliminary modeling of the friction stir welding process. *Proceedings of ICAWT*, EWI, Columbus, 1996, pp.297-310.
7. Mishraa R.S., Z.Y. Ma Friction stir welding and processing. Materials Science and Engineering R 50 (2005) pp. 1-78.
8. Marzoli, L., A. Von Stombeck, J.F. Dos Santos, C. Gambaro, M.L. Volpone and E. Rizzuto. Giunzioni di Al-CMM mediante Friction Stir Welding: influenza sulla distribuzione e sulle dimensioni delle particelle della fase dispersa. *29° Convegno Nazionale AIM, Modena*, Novembre, 2002.
9. Fernandez, G.J. and L.E. Murr. Characterization of tool wear and weld optimization in the friction-stir welding of cast aluminium 359+20% SiC metal-matrix composite. *Mat Charact,* 52 (2004), pp. 65-75.
10. Wert, J.A. Microstructures of friction stir weld joints between an aluminium-base metal matrix composite and a monolithic aluminium alloy. *Scripta Mat*, 49 (2003), p. 607.
11. He, H., N.N. Ekere and L. Cai. New statistic techniques for structure evaluation of particle packing. *Materials Science and Engineering*, A298 (2001), pp. 209-215.
12. Kanit, T., S. Forest, I. Galliet, V. Mounoury and D. Jeulin. Determination of the size of the representative volume element for random composites: statistical and numerical approach. *International Journal of Solids and Structures* 40 (2003), pp. 3647-3679.
13. Rhodes, C.G., M.W. Mahoney, W.H. Bingel, R.A. Spurling and C.C.

Bampton. Effects of friction stir welding on Microstructure of 7075 Aluminium. *Scripta Mat*, 36 (1997), p. 69.

14. Jata, K.V., S.L. Semiatin. Continuous dynamic recrystallization during friction stir welding of high strength aluminum alloys. *Scripta Mat*. 43 (2000), p. 743.
15. Leonard A.J. Microstructure and Ageing Behaviour of FSWs in Aluminium Alloys 2014AT651 and 7075-T651. *Proc. II Friction Stir Welding Symposium*. Goteborg, Sweden, 26-28 June (2000).
16. Gomez de Salazar J.M., M.I. Barrena. Role of Al_2O_3 particulate reinforcements on precipitation in 7005 Al-matrix composites. Scripta Mat. 2001 (44), pp. 2489-2495.
17. Bonollo, F., N. Gramegna and B. Molinas. Diecasting of aluminium matrix composites. Conf. Proc. 2nd Int. Conf. On HTDC, 21-22 April 2004, Brescia (Italy), pp. 361-366.
18. Liu, G., L.E. Murr, C.S. Niou, J.C. McClure and F.R. Vega. Microstructural aspects of the friction-stir welding of 6061-T6 aluminum. *Scripta Materialia*, 37 (1997), pp. 355-361.
19. Gutierrez-Urrutia I., M.A. Muñoz-Morris and D.G. Morris. The effect of coarse second-phase particles and fine precipitates on microstructure refinement and mechanical properties of severely deformed Al alloy *Materials Science and Engineering A, Volume 394, Issues 1-2 (2005),* pp. 399-410.
20. Q Su, J., T.W. Nelson, R. Mishra and M.Mahoney. Microstructural investigarion of friction stir welded 7050-T651 aluminum. *Acta Materialia*, 53 (2003), pp. 713-729.
21. Bhargava N., I. Samajdar, S. Ranganathan and M. Surappa. Role of Cold Work and SiC Reinforcements on the β'/β Precipitation in Al-10 pct Mg Alloy. *Metall. Trans*, 29A (1998), p. 2835.
22. Dutta I., C.P. Harper and G. Dutta. Role of Al_2O_3 Particulate Reinforcements on Precipitation in 2014 Al-Matrix Composites. *Metall. Trans*, 25A (1994), p. 1591.
23. Ferragut R., A. Somoza, A. Tolley and I. Torrioni. Precipitation kinetics in Al-Zn-Mg commercial alloys, *Journal of Materials Processing Technology*, 141 (2003), pp. 25-40.
24. Sutton M.A., A. P. Reynolds, B. Yang and R. Taylor. Mode I fracture and microstructure for 2024-T3 friction stir welds. *Materials Science and Engineering* A354 (2003), pp. 6-10.
25. Doel, T.J.A. and P. Bowen. Tensile properties of particulate-reinforced metal matrix composites. *Composites Part A: Applied Science and Manufacturing,* 27 (1996) pp. 655-665.
26. Mummery, P. and B. Derby. The influence of microstructure on the fracture behaviour of particulate metal matrix composites. *Mater. Sci. Eng.* A135 (1991) p. 221.
27. McHugh P.E., R.J. Asaro and C.F. Shih. Computational modeling of metal matrix composite materials-I. Isothermal deformation patterns in ideal microstructures. *Acta Metall. Mater.* 41 (1993) p. 1461.
28. Arsenault, R.J., N. Shi, C.R. Feng and L. Wang. Localized deformation of SiC-Al composites. *Mater. Sci. Eng.* A131 (1991) pp. 55-68.
29. Song S.G., N. Shi, G.T. Gray III and J.A. Roberts. Reinforcement Shape Effects on the Fracture Behavior and Ductility of Particulate-Reinforced 6061-Al Matrix Composites. *Metall. Mater. Trans.* A27 (1996) p. 3739.
30. Qin S., C. Chen, G. Zhang, W. Wang and Z. Wang, The effect of particle shape on ductility of SiCp reinforced 6061 Al matrix composites, *Materials Science and Engineering A272* (1999), pp. 363-370.
31. Li, Z., A.M. Samuel, F.H. Samuel, C. Ravindran, H.W. Doty and S. Valtierra. Parameters controlling the performance of AA319-type alloys, Part II. Impact properties and fractography. *Mat Sci and Eng* A 367 (2004), pp. 111-122.
32. Srivatsan, T.S. and A. Prakash. The quasi-static fracture behavior of an aluminum alloy metal matrix composite. *Composites Sci and Techn*, 54 (1995), pp. 307-315.
33. Srivatsan, T.S. and M. AL-Hajri. The fatigue and final fracture behavior of SiC particle reinforced 7034 aluminum matrix composites. *Composites, Part B: Engineering*, 33 (2002), p. 391.
34. Srivatsan T.S., Al-Hajri, Meslet, M. Petraroli, B. Hotton, P.C. Lam. Influence of silicon carbide particulate reinforcement on quasi static and cyclic fatigue fracture behavior of 6061 aluminum alloy composites. *Mat Sci and Eng* A325 (2002), pp. 202-214.
35. Wang Z.G., S. Li, L. Sun. Fatigue and fracture behaviors of discontinuously reinforced aluminum matrix composites. *Key Engineering Materials*, 104-107 (1995), pp. 729-748.
36. Boromei I., Ceschini L., Minak G., Morri A., Tarterini F., Microstructure, tensile and fatigue properties of AA6061/20vol.%Al_2O_{3p} Friction Stir Welded joints. In press on *The Special Issue of Composite a Journal*.